Water Resources Management
https://doi.org/10.1007/s11269-023-03617-7

Detecting Background Leakages in Water Infrastructure With Fiber Optic Distributed Temperature Sensing: Insights From a Heat Transfer-Unsaturated Flow Model

Andrea D'Aniello[1]

Received: 30 May 2023 / Accepted: 12 September 2023

Abstract
The use of fiber optic distributed temperature sensing (DTS) to detect and locate leaks is still in its infancy in water infrastructure, despite its promising capabilities. Only few experiments tested this technology, and none of these studies focused on small but persistent leaks, like background leakages, which are ubiquitous and generally go undetected with the technology currently available, thus posing a serious threat to the available water resource. To test the feasibility of detecting and locating background leakages with fiber optic DTS, this study provides a detailed analysis on flow and temperature alterations around leaking water pipelines in presence of small leaks (5, 25, and 125 L/d) with small to moderate temperature differences with the surrounding soil, under 3 different pipe defect configurations, either in absence or in presence of pipe thermal insulation. Transient 3D heat transfer-unsaturated flow numerical simulations showed that there is potential to use temperature alterations to detect and locate incredibly small leaks with fiber optic DTS, like background leakages, despite the influence of pipe temperature on the surrounding soil. The analysis showed that extent, distribution, and magnitude of these alterations are convection dominated at a given temperature difference between leaked water and undisturbed soil, and that it may not be strictly necessary to place the optical fiber directly below the pipe. Indeed, optical fibers located within the utility trench at the sides of the pipe and below its bottom showed comparable or even better performance, thus giving new opportunities to retrofit existing pipelines as well.

Keywords Pipe leakage · Distributed temperature sensing (DTS) · Optical fibers · Leak detection and location · Utility trench · Unsaturated zone

1 Introduction

Detecting, locating, and reducing leaks is easier said than done in today's water infrastructure. Countless researchers and practitioners have given their contribution to the topic, but many governments and water utilities are still somehow reluctant or unable to invest money and resources to systematically tackle this problem, despite the urgency.

✉ Andrea D'Aniello
andrea.daniello@unina.it

[1] University of Naples Federico II, Department of Civil, Architectural and Environmental Engineering, via Claudio 21, 80125 Napoli, Italy

Figures are impressive: 126 billion m^3/yr (346 million m^3/d) is the recent estimate of the global non-revenue water, with an estimated financial cost of USD 39 billion/yr (Liemberger and Wyatt 2019). But the problem is not 'merely' financial. This massive amount of water lost could serve the current and future needs of millions of people and could have a tremendous social impact worldwide, especially for the communities struggling every day for a safe and easy access to drinking water. Water scarcity and droughts are exacerbated by leaking water utilities as more water needs to be extracted, thus contributing to the depletion of natural freshwater resources (FAO 2012). Inevitably, this leads to higher energy demands by pumping stations and treatment plants, the use of more chemicals for water treatment, and the increase of greenhouse gases emissions (FAO 2012; Stokes et al. 2014). Despite leaked water can potentially recharge urban aquifers (Lerner 1986, 1990, 2002; Price and Reed 1989; Foster 2001; Hibbs and Sharp 2012; Bhaskar et al. 2016; Han et al. 2017), its actual reuse is limited as urban soils and groundwaters may host a variety of contaminants (Tubau et al. 2017). Large volumes of wastewater and stormwater are lost from leaking sewers as well (Chisala and Lerner 2008), thus contributing to the spread of harmful contaminants beneath urban environments (Wakida and Lerner 2005; Vázquez-Suñé et al. 2005; Tubau et al. 2017; Burri et al. 2019). Furthermore, this unintentional recharge may create dangerous interactions between urban aquifers and the intricate system of shallow and deep anthropogenic features within the subsurface (e.g., building basements, tunnels, underground constructions, utility pipelines, utility trenches, etc.), potentially causing serious adverse effects, like flooding of underground spaces, foundations corrosion, excessive hydrostatic stress, and structures uplift (Vázquez-Suñé et al. 2005; Attard et al. 2016). Leaking pipes can also produce sinkholes, which may lead to dangerous road pavement collapses and foundation settlements (Waltham et al. 2005). Indeed, this is not sustainable.

Generally, performance targets drive water companies and managing authorities primarily towards reducing leaks in water supply infrastructure. As a result, numerous technologies and algorithms for leak detection and location are specifically tailored for water distribution networks. Reported and unreported leakages, typically bursts and high flow rate leaks (in the order of m^3/h), are addressed the most (Lambert et al. 2015a; Li et al. 2015; Adedeji et al. 2017; Hu et al. 2021), as their occurrence is followed by detectable feedback from the network, like sudden flow rate increase, pressure drops, and acoustic anomalies. However, a large amount of water is actually lost through background leakages, especially in well-managed infrastructure (Lambert et al. 1999; Lambert and McKenzie 2002; Lambert 2009; Lambert et al. 2015a, b). Although relatively small (in the order of L/d), these leaks are ubiquitous throughout the network and run continuously. Despite their sensitivity to pressure, background leakages are not associated to any appreciable pressure drop or acoustic anomaly, therefore they give practically no feedback, going undetected for a very long time and posing a serious threat to the available water resource.

Nonetheless, the soil/trench filling material surrounding such persistent leaks could be somehow affected. If a sufficient temperature difference exists between water flowing within the pipes and the subsurface, a temperature alteration may arise in proximity to the leaks, and this information could be retrieved to detect and locate them. Since leaks occurrence and location are unknown, an unfeasible number of discrete temperature sensors would be required to monitor kilometers long pipelines. A viable alternative would require a very long sensor running along the entire length of the pipeline and able to detect these anomalies with a reasonable temperature and spatial resolution. In this regard, distributed fiber optic sensors could be the best option currently available, as every point along the fiber acts a sensing element, potentially offering a continuous and fast monitoring of strain, temperature, and vibration over tens of kilometers (Motil et al. 2016; Wijaya et al. 2021).

Furthermore, fiber optic cables are very thin and low weight, can be attached to almost any surface, have a long-term durability, are insensitive to humidity, corrosion, and electromagnetic interferences, and can work under very harsh conditions, sustaining a wide range of temperatures and pressures (Niklès et al. 2004; Motil et al. 2016; Wijaya et al. 2021). These characteristics made them suitable for a variety of environmental and structural health monitoring applications, including leak detection and location in oil, gas, and liquid pipelines (Niklès et al. 2004; Inaudi et al. 2008; Bolognini and Hartog 2013; Wang et al. 2017; Drusová et al. 2021; Wijaya et al. 2021).

The use of fiber optic distributed temperature sensing (DTS) is still in its infancy in water distribution networks (Ibrahim et al. 2021), despite the promising capabilities of the technology (fundamentals on the operating principles of DTS techniques can be found in Niklès et al. 2004, Inaudi et al. 2008, and Wijaya et al. 2021). Only few lab and field scale experiments tested this technology for detecting and locating leaks by monitoring temperature anomalies around water pipelines (Lombera et al. 2014; Xu et al. 2020; Wang et al. 2022). Although successful, these tests put much of the emphasis on the capabilities of the specific sensing technique to detect a temperature anomaly, and practically none on the flow and temperature response in the surrounding soil/trench filling material. Some efforts in this regard were made by Jacobsz and Jahnke (2020) with a long-term field scale experiment, although the main purpose of their study was to explore the performance of discrete fiber optic sensors (fiber Bragg gratings) to monitor both strain and temperature anomalies as a means for leak detection.

Up to now, a detailed analysis on flow and temperature alterations around leaking water pipelines buried in the subsurface is missing, especially for small leaks with small to moderate temperature differences with the surrounding soil/trench filling material. This study is the first to provide this since the first occurrence of the leaks in a controlled, yet realistic, numerical environment. The goal is to test the feasibility of detecting and locating background leakages with fiber optic distributed temperature sensing, so as to provide theoretical and practical insights to support future field scale experiments and applications.

2 Methodology

2.1 Conceptual Model

A leaking water pipeline laid in a utility trench together with fiber optic sensing cables forms the core of the conceptual model (Fig. 1). The utility trench is then surrounded by native soil hosting an unconfined aquifer (at 1 m from the bottom of the trench). As the aim is to assess the ability of the optical fibers to detect small leaks with small to moderate temperature differences with the surrounding soil/trench filling material, the time frame of the simulations is set to 4 days, which is sufficient to fully observe flow and temperature alterations in proximity to the sensing cables since their first occurrence.

The pipe is representative of a pressurized water distribution main leaking from one of its joints. This configuration was preferred compared to others (e.g., wastewater and stormwater pipelines) as more information is readily available on real losses. However, as water flow within the pipe is not modeled, the conceptual model is potentially representative of any type of water infrastructure. Therefore, the pipe material is not specified, and its diameter is just indicative. To reproduce different defects, the leaks can occur from i) the entire length, ii) the upper right quarter, or (iii) the lower right quarter of the joint, located at the middle of

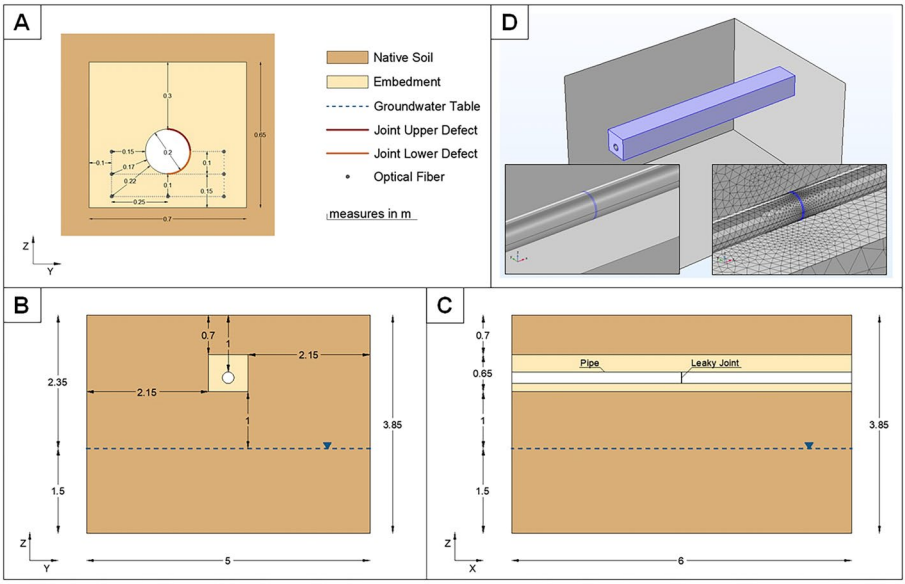

Fig. 1 Detail of the utility trench with leaking pipe and optical fibers (**A**), YZ (**B**) and XZ (**C**) plane views of the conceptual model, and model domain with computational mesh around the leaking joint (**D**). Dotted lines in panel (**A**) are used to better identify the optical fibers located at the spring line, at the bottom of the pipe, and below its bottom

the pipeline (Fig. 1). Leak rates of 5, 25, and 125 L/d were chosen to reproduce small leaks of long duration (i.e., background leakages), which generally go undetected and are responsible for large amounts of water lost (Lambert et al. 1999; Lambert and McKenzie 2002; Lambert 2009; Lambert et al. 2015a, b).

In most scenarios, the pipe has no thermal insulation, as generally occurs in practice. Therefore, the outer surface of the pipe is assumed at the same temperature of water flowing inside it, namely 1, 3, or 5 °C higher than the undisturbed soil (i.e., at a sufficient distance from the pipe where it is not affected by its temperature), set at 12.5 °C. This is a reasonable approximation as heat transfer in pipe-soil systems is generally convection dominated, given the typical velocity ranges of water in the pipes and the small thickness of these (Milano 2012). Furthermore, as the portion of the pipeline analyzed in the present model is limited (6 m) and its top lays at a depth of 1 m from the ground surface (Fig. 1), the effects of surface temperature daily fluctuations can be considered negligible (Wu and Nofziger 1999; Milano 2012). These effects are disregarded for the entire model as well, given that they would only affect the very first few tens of centimeters from the ground surface over the short time frame considered. Therefore, pipe temperature is kept constant throughout the simulations, and the same applies to leaked water at the joint defects. As such, in absence of thermal insulation, pipe temperature inevitably affects its surroundings, and to account for its influence on soil temperature, flow and temperature fields are computed up to a steady state condition prior to the onset of the leaks (Sec. 2.3; for these scenarios, soil temperature distributions prior to the onset of the leaks can be found in the Supplementary material). In a few illustrative scenarios, the effects of thermal insulation are also analyzed. In this case, the outer surface of the pipe is assumed at the same temperature of the undisturbed soil and leaked water is just 1 °C higher, whereas leaks occur over the entire joint.

The configuration of the utility trench (Fig. 1) reflects the combination of the design guidelines of different countries and is meant to be suitable for both rigid and flexible pipes (Howard 1996; Milano 2012; Yorkshire Water 2018). The portion of trench backfill where the pipe is laid (i.e., the embedment) is filled with a cohesionless free draining material (sand/gravel), while the remaining of the trench is filled with native soil (therefore, not depicted in Fig. 1), as commonly done in practice (Howard 1996; Milano 2012; Yorkshire Water 2018). To have enough contrast with the trench filling material, a sandy clay loam (USDA SCS 1987) is chosen as native soil.

The sensing cables run all along the pipe and are placed at different locations within the trench to assess which of these would be the most suitable for an early detection of the modeled leaks. The optical fibers are deployed on both sides of the pipe, two at the spring line (i.e., the horizontal centerline of the pipe), two at the bottom of the pipe, and three below its bottom, for a total of seven (Fig. 1). No sensing cable is placed over the pipe as leaked water eventually flows downwards, and leaks occurring at the bottom half of the pipe would be most likely missed. The optical fibers are also placed at distance from the pipe and the sides of the trench to reduce the effects of pipe and native soil temperature on the sensing cables, while keeping in mind the feasibility of their installation for both existing and new pipes. As fiber optic cables are generally really thin, from few millimeters to roughly a centimeter including all their components (i.e., core, cladding, inner coating, strength member, and outer jacket), they are not expected to have any appreciable influence on the flow and heat transfer mechanisms modeled here. Therefore, no size or type specifications are provided for the optical fibers. Furthermore, as the conceptual model aims to be as general as possible, it is not meant to explore the performance of specific sensing techniques (e.g., Raman or Brillouin), hence, this information is not provided. To reproduce spatial resolutions typical of DTS systems used for kilometers long applications, the modeled temperature alterations are then averaged along the fibers over three different lengths centered at the leaky joint, namely 1, 0.5, and 0.2 m (Inaudi et al. 2008; Motil et al. 2016; Wang et al. 2022). Finally, as in these sensing systems temperature resolutions commonly vary from 0.1 to 0.01 °C (Inaudi et al. 2008; Drusová et al. 2021; Wang et al. 2022), leak detection thresholds are set to 0.1 and 0.5 °C.

2.2 Outline of the Simulations

A total of 30 scenarios were modeled, and a summary is provided hereinafter. When the pipe is not thermally insulated (27 scenarios), 3 joint defects (entire length, upper right quarter, and lower right quarter of the joint, denoted by letters J, U, and L) suffer leaks of 5, 25, and 125 L/d (denoted as L5, L25, and L125), with pipe and leaked water temperature of 1, 3, and 5 °C higher than the undisturbed soil (denoted as T1, T3, and T5). In presence of thermal insulation (3 scenarios, denoted by the letter I), the pipe leaks from the entire length of the joint (J) with leak rates as above (L5, L25, and L125) and a temperature of leaked water of 1 °C higher than the undisturbed soil (T1). All scenarios are time dependent (i.e., transient), and the simulation time is set to 4 days.

2.3 Numerical Modeling

The scenarios were modeled with COMSOL Multiphysics® version 6.0.0.405 (COMSOL 2021), which solves the governing equations of unsaturated flow and heat transfer in

porous media by the finite element method (the mathematical formulation of these equations is reported in the Appendix). Given the high nonlinearity of the transient problem, a mass lumping procedure (Istok 1989) was enforced for the numerical solution of the governing equations of unsaturated flow. The model domain is sufficiently big (6 m×5 m×3.85 m, Fig. 1) to avoid potential interactions between leaked water and boundary conditions, and the numerical mesh consists of 438′836 irregular tetrahedra, refined at the leaky joint and within the utility trench, with element sizes ranging between 1.75 and 29.4 cm. The time step depends on convergence history, although its maximum is set to 1 h to have a sufficiently fine temporal discretization even when the flow originating from the joint defects is fully developed. Convergence is reached when the solution of the nonlinear solver respects a relative tolerance of 0.01. Each scenario took about 4 to 14 h of calculations on an Intel®Core™ i9-8950HK CPU running at 2.9 GHz with 16 GB RAM, for a total runtime of about 223 h.

Boundary conditions are presented in Table 1. In all scenarios, a no flux boundary condition is enforced for the outer surface of the pipe (except for the joint defects) and for the top of the domain, whereas a fixed hydraulic head is set for the bottom and the lateral boundaries to reproduce a static groundwater table at 1.5 m from the bottom of the domain. Top and bottom of the model are set at a fixed temperature of 12.5 °C, whereas a no heat source condition is applied to the lateral boundaries. The leaky joint is modeled as a 1 cm long portion of the outer surface of the pipe over which a flux boundary condition is enforced to reproduce leak rates of 5, 25, and 125 L/d, and the temperature is fixed to 13.5, 15.5, and 17.5 °C, depending on the scenario. Instead, when the defects occur at the upper or at the lower right quarter of the joint, the flux and the temperature boundary conditions are applied only to the selected quarter of this 1 cm long portion of the outer surface of the pipe. To avoid model instabilities induced by abrupt changes in the flow field at the leaky joint, leak rates are set to increase linearly up to the selected value during the first day, and then are kept constant for the remaining three days. When the pipe has no thermal insulation, the temperature of the pipe outer surface is fixed to the value at the leaky joint, whereas a no heat source condition is enforced if the pipe is thermally insulated. For each scenario, initial conditions prior to the onset of the leaks are obtained by running a steady state simulation to reach an equilibrium state consistent with the boundary conditions, assuming a hydraulic head of 1.5 m and a temperature of 12.5 °C for the whole domain as initial guess for the nonlinear solver.

Table 1 Boundary conditions

Boundary	Boundary Conditions	
	Pipe without thermal insulation	Pipe with thermal insulation
Top	no flux fixed temperature [12.5 °C]	no flux fixed temperature [12.5 °C]
Sides	fixed hydraulic head [1.5 m] no heat source	fixed hydraulic head [1.5 m] no heat source
Bottom	fixed hydraulic head [1.5 m] fixed temperature [12.5 °C]	fixed hydraulic head [1.5 m] fixed temperature [12.5 °C]
Pipe outer surface	no flux fixed temperature [13.5, 15.5, or 17.5 °C]	no flux no heat source
Pipe defects	flux [5, 25, or 125 L/d] fixed temperature [13.5, 15.5, or 17.5 °C]	flux [5, 25, or 125 L/d] fixed temperature [13.5, 15.5, or 17.5 °C]

Soil hydraulic and thermal properties are listed in Table 2. Instead, to reproduce the temperature dependency of fluid properties (i.e., density, dynamic viscosity, specific heat at constant pressure, and thermal conductivity), the data provided by The Engineering ToolBox (2001) were interpolated with simple polynomial expressions and then incorporated within the numerical model. Fluid properties pressure dependency is here neglected as pressure alterations are too low in the modeled scenarios to result in any appreciable variation of these properties.

3 Results

3.1 Leaked Water Flow Behavior

As the leaks occur, leaked water initially occupies the pore spaces of the embedment in the close vicinity of the pipe defects and gradually spreads within the utility trench, thus resulting in a localized increase in the effective water saturation (Appendix). However, this spreading is limited as leaked water soon finds its way out of the embedment, preferentially moving downwards within the native soil. This eventually occurs in all scenarios, regardless of the leak rate. Although this may seem unexpected given that the embedment has an intrinsic permeability of roughly 1.4 orders of magnitude higher than the native soil (Table 2), an explanation to this behavior is to be found in the soil retention properties (specifically, α and n van Genuchten parameters; Table 2). Briefly, as water within the unsaturated zone is initially in equilibrium with the static groundwater table (i.e., a hydrostatic pressure distribution exists), prior to the onset of the leaks the distribution of the effective water saturation along the vertical follows the van Genuchten retention curve (Appendix). However, a sharp discontinuity exists in the effective water saturation at the interface between the embedment and the native soil, despite pressure being the same. This occurs because the retention properties of the embedment differ from the native soil. As these properties are higher in the embedment, here the effective water saturation is much lower than in the native soil (about

Table 2 Soil properties

Parameter	Embedment	Native Soil
[a]θ_r – Residual water content [m^3/m^3]	0.045	0.1
[a]θ_s – Saturated water content [m^3/m^3]	0.43	0.39
[a]van Genuchten α parameter [1/m]	14.5	5.9
[a]van Genuchten n parameter	2.68	1.48
[a]k – Intrinsic permeability [m^2]	$9.591 \cdot 10^{-12}$	$4.230 \cdot 10^{-13}$
[b]ρ_s – Solid phase density [kg/m^3]	2000	1900
[b]c_s – Solid phase specific heat [J/(kg•K)]	729.9	817.3
[b]k_s – Solid phase thermal conductivity [W/(m•K)]	0.4	0.64
[c]λ_l – Longitudinal thermal dispersivity [m]	0.5	0.5
[c]λ_t – Transverse thermal dispersivity [m]	0.05	0.05

[a]Carsel and Parrish (1988)

[b]Dalla Santa et al. (2020)

[c]Diersch (2014)

0.011 compared to 0.42 at the bottom of the trench), and the relative permeability (Appendix) is even lower (about $2.48 \cdot 10^{-8}$ compared to $3.24 \cdot 10^{-4}$ at the bottom of the trench). Therefore, the resulting hydraulic conductivity (Appendix) of the embedment is so low compared to the native soil to make water flow less likely within the trench, and leaked water preferentially moves downwards in the native soil, supported by gravity. For more details regarding this peculiar behavior, the interested reader is addressed to D'Aniello et al. (2021, 2022).

Although the fate of leaked water is pretty much the same among the scenarios, a few differences arise in the migration pathway as the configuration of the pipe defects changes, the leak rate increases, and the temperature difference between leaked water and the undisturbed soil varies (Fig. 2; Supplementary material). Indeed, while the plume of leaked water is symmetric when the entire joint is leaking, it is not when the leaks occur at the upper or at the lower right quarter of the joint. This asymmetry is more evident in the embedment rather than in the native soil, where it reduces as the leak rate increases. When the leaks occur at the upper right quarter of the joint, the effective water saturation increases more at this location and on the right side of the embedment. As the leak rate increases, more water reaches the lower left side of the embedment both from below and over the pipe, thus increasing the effective water saturation in this location as well. However, the lower left side in the close vicinity of the pipe is only slightly affected by the leaks. Instead, when the leaks occur at the lower right quarter of the joint, leaked water reaches the left side of the embedment only from below the pipe. Although the effective water saturation below the bottom of the pipe is overall higher in these scenarios, the embedment shows no to very small variations in its effective water saturation over the bottom of the pipe on the left side and, in general, over the spring line. Furthermore, when the leaks occur at the upper or at the lower right quarter of the pipe, the effective water saturation is slightly higher at the pipe defects than when the entire joint leaks. This occurs because the leak rate is the same but the surface over which the leaks occur reduces, therefore the flux is locally higher and so is the pressure, thus resulting in higher effective water saturation (the pressure–saturation relationship is described in the Appendix). Overall, the extent of the plume of leaked water in the native soil does not change much among the different pipe defect scenarios, and these small differences further reduce as the leak rate increases. Furthermore, as expected a leak rate increase is followed by an overall increase in the extent of the plume of leaked water and in the effective water saturation. Small differences arise among the scenarios also because of the temperature difference between leaked water and the surrounding soil. In particular, the lower this difference, the higher the effective water saturation. Indeed, as the temperature of leaked water increases from 13.5 to 15.5 and 17.5 °C, water viscosity reduces of about 2.5%, 7.4%, and 12% compared to the undisturbed native soil (at 12.5 °C), whereas water density variations are practically negligible (below 0.1%). As a result, the hydraulic conductivity is overall higher as the temperature increases, and a lower effective water saturation is required to let the same amount of leaked water flow within the soil.

Finally, there is practically no difference in migration pathway and distribution of leaked water between the scenarios with and without thermal insulation of the pipe. Indeed, despite the different initial conditions (Table 1), the maximum modeled temperature difference (1 °C) when the pipe is thermally insulated (Supplementary material) is so low to cause no appreciable changes in fluid properties and, in turn, no variations in the flow field.

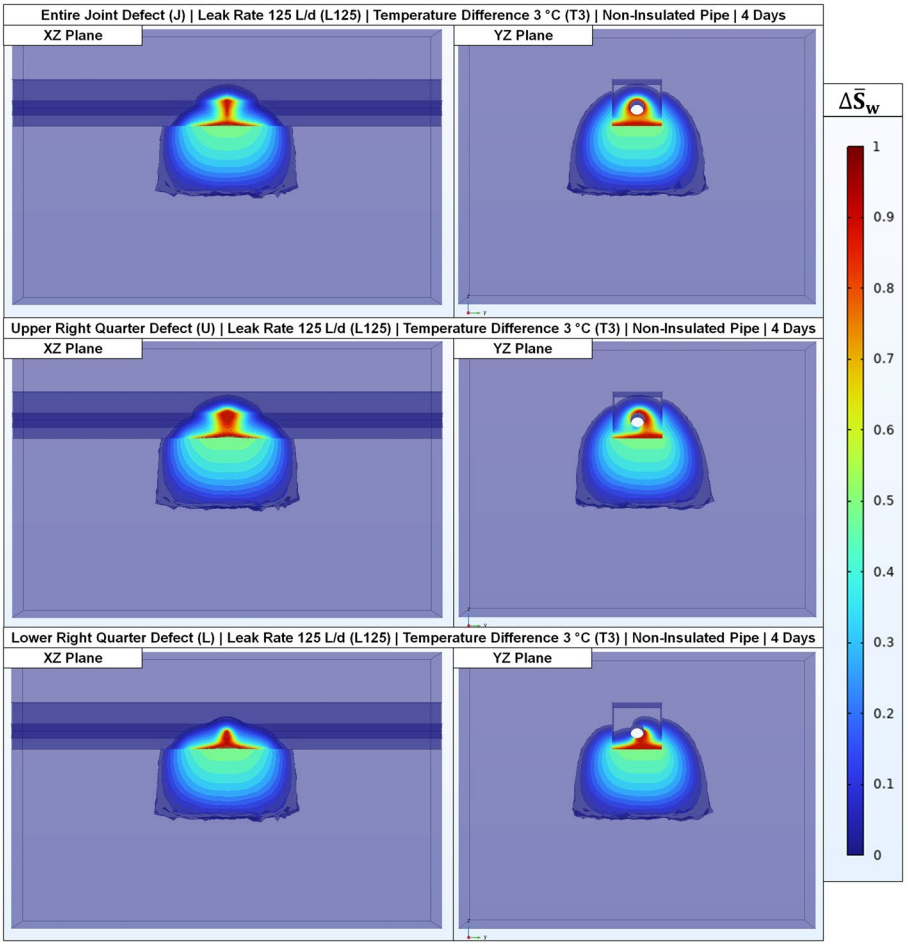

Fig. 2 Predicted distribution of the effective water saturation variation at 4 days with respect to the initial conditions ($\Delta\bar{S}_w$) for all pipe defect configurations (J – entire joint defect, U – upper right quarter joint defect, L – lower right quarter joint defect), leak rate of 125 L/d (L125), temperature difference of 3 °C between leaked water and undisturbed soil (T3), and non-insulated pipe. Transparent colors are used to display the results within the numerical domain. All separate outputs are available in the Supplementary material together with those of the remaining scenarios

3.2 Temperature Alterations Induced By the Leaks

Extent, distribution, and magnitude of temperature alterations are convection dominated at a given temperature difference between leaked water and the undisturbed soil. Indeed, the temperature plumes resulting from the leaks (Fig. 3; Supplementary material) are similar in shape to those of leaked water (Fig. 2; Supplementary material), and mostly follow the alterations to the flow field induced by the leaks. Furthermore, as the leak rate increases, extent and magnitude of temperature alterations increase as well. As expected, the magnitude of these alterations increases as the temperature of leaked water increases, while extent and distribution remain the same for a given leak rate and pipe defect configuration.

Besides of the pipe defects location, which inevitably affects the overall flow field (Sec. 3.1), the distribution of temperature alterations strongly depends on whether the pipe is thermally insulated or not. Indeed, even at a very low leak rate (5 L/d) and a small temperature difference (1 °C), the temperature contrast between leaked water and the surrounding soil is much more evident at the leaks when the pipe is thermally insulated, as it is at its maximum here. As expected, around the pipe these alterations increase with time and with increasing leak rate and decrease at distance from the leaky joint (Figs. 3 and 4; Supplementary material).

Conversely, this contrast is indeed lower when the pipe is not thermally insulated. In absence of thermal insulation, the magnitude of temperature alterations increases moving

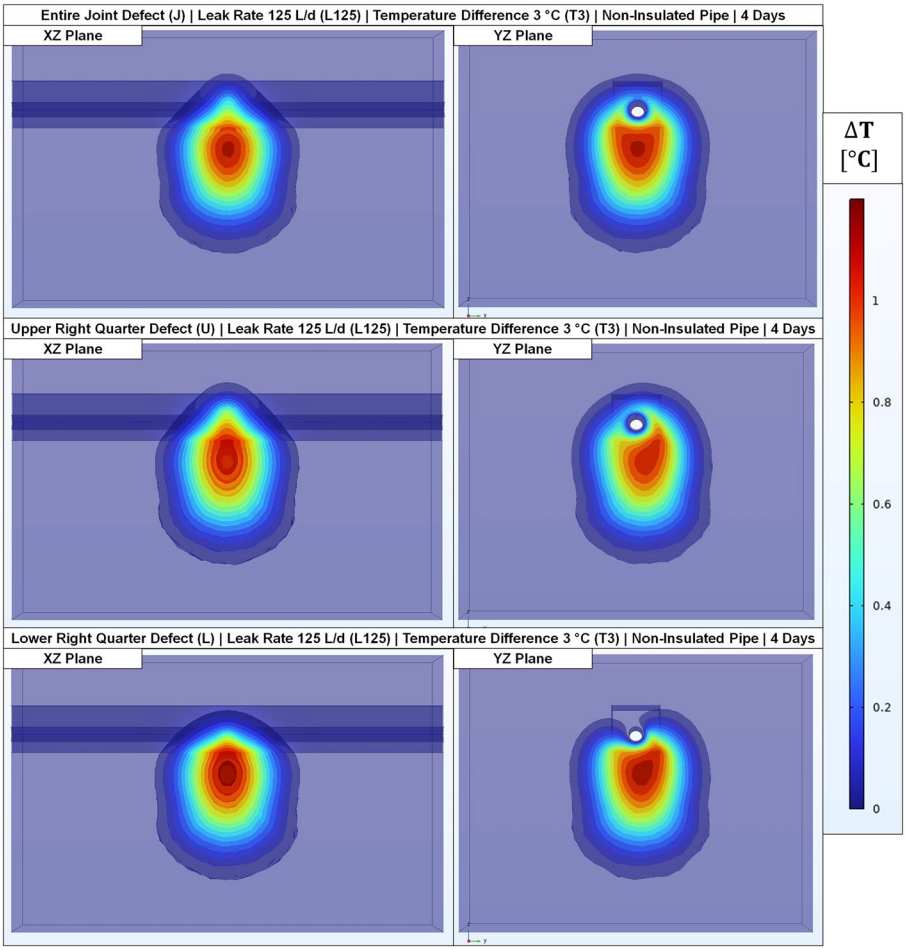

Fig. 3 Predicted distribution of temperature alterations at 4 days with respect to the initial conditions (ΔT) for all pipe defect configurations (J – entire joint defect, U – upper right quarter joint defect, L – lower right quarter joint defect), leak rate of 125 L/d (L125), temperature difference of 3 °C between leaked water and undisturbed soil (T3), and non-insulated pipe. Transparent colors are used to display the results within the numerical domain. All separate outputs are available in the Supplementary material together with those of the remaining scenarios

away from the pipe in the main flow direction (i.e., downwards) as the effects of pipe temperature on the surrounding soil reduce with distance (Fig. 3; Supplementary material). In these scenarios, the maximum temperature difference between leaked water and the surrounding soil is located below the pipe and moves downwards as the flow develops.

However, a closer inspection at the close vicinity of the pipe may help reveal that noticeable temperature alterations can arise at this location as well despite the influence of pipe temperature (Figs. 5 and 6; Supplementary material). Although small (around 0.1 °C at 4 days) when the leak rate is at its minimum (5 L/d) and the temperature difference between leaked water and the undisturbed soil is the lowest (1 °C), these alterations might become detectable as the leak rate increases (up to roughly 0.2 and 0.3 °C at 25 and 125 L/d at 4 days), assuming a sufficiently fine temperature and spatial resolution of the sensing system (Sec. 3.3) and a low detection threshold. As the temperature difference with the undisturbed soil increases up to 3 and 5 °C, these alterations become indeed more relevant in proximity to the pipe, up to roughly 0.3 and 0.5 °C at 4 days for the considerably low leak rate of 5 L/d, and up to 1–1.5 °C for the leak rate of 125 L/d. This is indeed promising if compared to the detection thresholds of 0.1 and 0.5 °C (Sec. 2.1) and considering that these leak rates are representative of background leakages.

Despite overall a steady state in not reached, temperature alterations in proximity to the leaks tend to get close to it within the time frame considered (4 days), since temperature changes reduce significantly over the end of the simulations (Figs. 4, 5 and 6; Supplement ary material) as a consequence of a flow field almost fully developed at this location. In all scenarios without thermal insulation, at 4 days predicted temperature alterations below the bottom of the pipe (at 10 cm) are always higher than at the bottom, followed by those at the spring line. This is not always true since the very beginning of the leaks, depending on the pipe defect configuration and on the leak rate. Indeed, temperature alterations can be locally higher either at the bottom of the pipe (lower pipe defects) or at the spring line (upper pipe defects) in the first stages of the leak. Temperature alterations are symmetric in the transversal direction (Y axis cut lines at the joint; Fig. 5; Supplementary material) when the entire joint leaks, and two peaks form at the sides of the pipe, except below its bottom when the leak rate is the lowest (5 L/d). Over time, two peaks form at the sides of

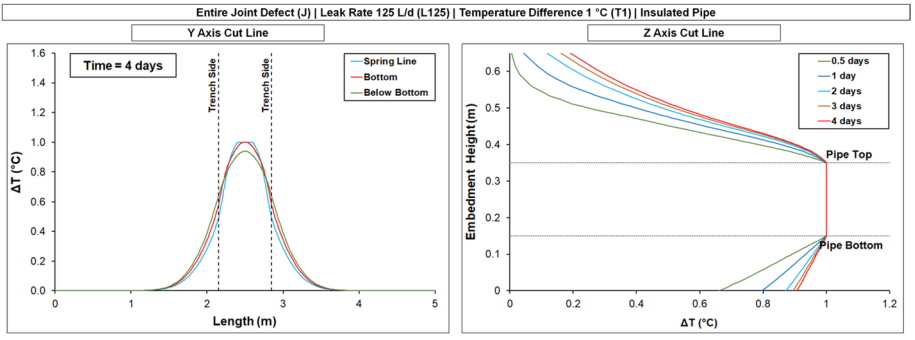

Fig. 4 Predicted distribution of temperature alterations with respect to the initial conditions (ΔT) along the Y axis cut lines at the joint (left) passing through the spring line, the bottom of the pipe, and 10 cm below the bottom of the pipe, and along the vertical centerline of the pipe passing through the joint (Z axis cut line at the embedment, right) for the entire joint defect configuration (J), leak rate of 125 L/d (L125), temperature difference of 1 °C between leaked water and undisturbed soil (T1), and insulated pipe (I). All separate outputs are available in the Supplementary material together with those of the remaining scenarios

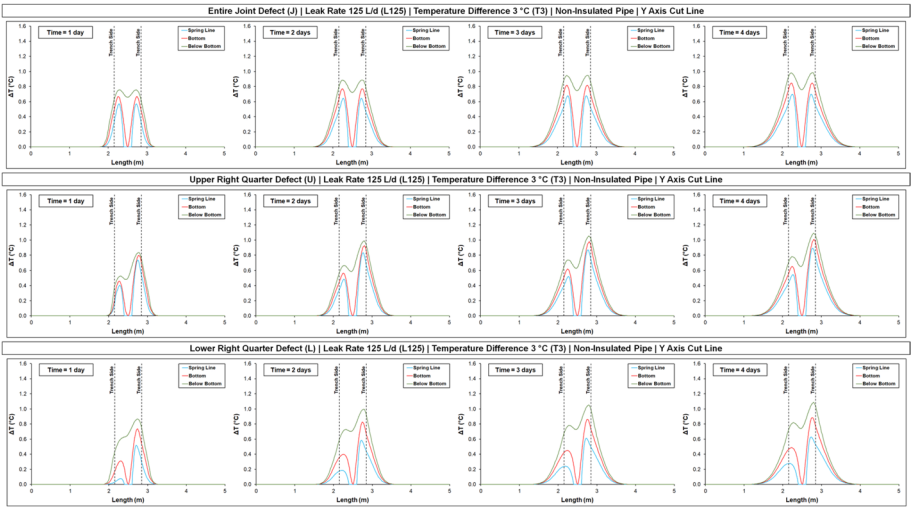

Fig. 5 Predicted distribution of temperature alterations with respect to the initial conditions (ΔT) along the Y axis cut lines at the joint passing through the spring line, the bottom of the pipe, and 10 cm below the bottom of the pipe for all pipe defect configurations (J – entire joint defect, U – upper right quarter joint defect, L – lower right quarter joint defect), leak rate of 125 L/d (L125), temperature difference of 3 °C between leaked water and undisturbed soil (T3), and non-insulated pipe. All separate outputs are available in the Supplementary material together with those of the remaining scenarios

the pipe in the other defect configurations as well, although as expected the peak is always higher at the right side. In all scenarios, these peaks move towards the sides of the trench in the transversal direction as the leak rate increases and the time progresses. Consistently with the flow field, temperature alterations on the left side are higher when the pipe leaks at its upper right quarter than at its lower right quarter, although both are lower than when the entire joint leaks. Along the vertical centerline of the pipe passing through the joint (Fig. 6; Supplementary material), temperature alterations below the pipe are always higher when the leaks occur at the lower right quarter and from the entire joint, whereas over the pipe these alterations are higher when the pipe leaks at the upper right quarter and are practically negligible when the leaks occur at the lower right quarter. Below the pipe,

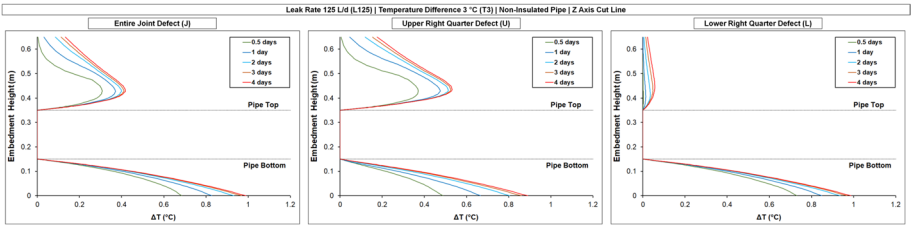

Fig. 6 Predicted distribution of temperature alterations with respect to the initial conditions (ΔT) along the vertical centerline of the pipe passing through the joint (Z axis cut line at the embedment) for all pipe defect configurations (J – entire joint defect, U – upper right quarter joint defect, L – lower right quarter joint defect), leak rate of 125 L/d (L125), temperature difference of 3 °C between leaked water and undisturbed soil (T3), and non-insulated pipe. All separate outputs are available in the Supplementary material together with those of the remaining scenarios

temperature alterations increase downwards, whereas moving upwards over the pipe these reach a maximum roughly at 5–10 cm (the higher the leak rate, the farther the peak location) and then decrease.

3.3 Temperature Alterations At the Optical Fibers

Over time, temperature alterations at the seven optical fibers located in proximity to the pipe (Fig. 1) follow an S-shaped curve (Figs. 7, 8, 9 and 10; Supplementary material). These curves become steeper and higher as the temperature of leaked water and the leak rate increase, since the magnitude of temperature alterations induced by the leaks strongly depends on these two parameters (Sec. 3.2). Indeed, as the optical fibers are located at distance from the pipe, once the leaks occur no alteration is immediately recorded at the sensing cables. Temperature alterations occurrence at the optical fibers depend on their location with respect to the pipe defect and on the leak rate. The closer the optical fiber is to the defect and the higher the leak rate, the faster temperature alterations occur at these locations. As the entire joint leaks, the optical fiber located below the bottom of the pipe along the vertical centerline (referred to as "Below Bottom – Middle" in Figs. 7 to 10 and in the Supplementary material) is generally the first to witness a temperature alteration, followed by the others below the bottom, at the bottom, and at the spring line. When the leaks occur at the defects on the right side of the pipe, the optical fibers located here experience

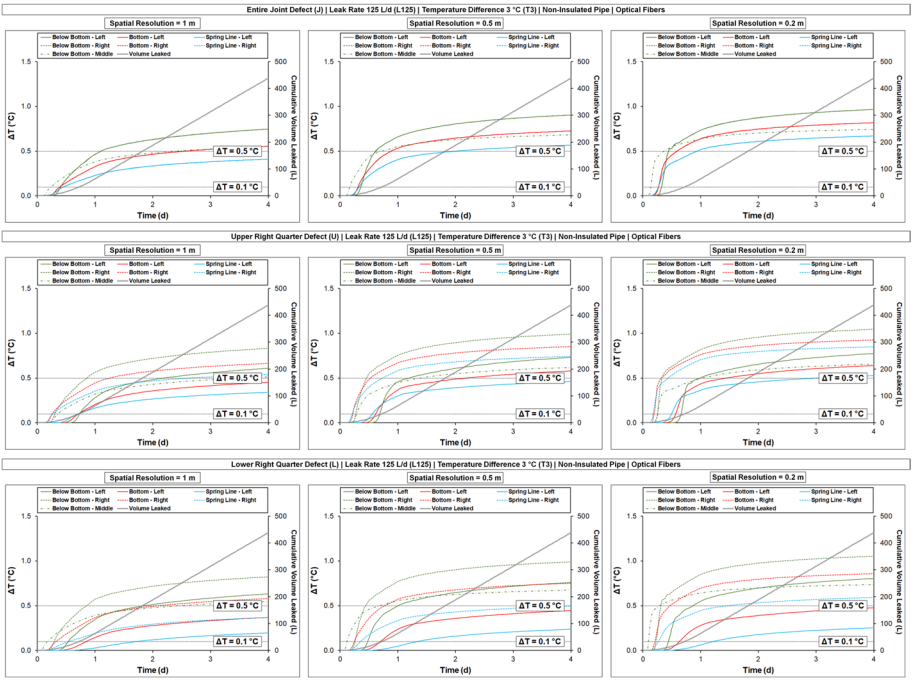

Fig. 7 Predicted temperature alterations over time with respect to the initial conditions (ΔT) at the optical fibers for all pipe defect configurations (J – entire joint defect, U – upper right quarter joint defect, L – lower right quarter joint defect), leak rate of 125 L/d (L125), temperature difference of 3 °C between leaked water and undisturbed soil (T3), non-insulated pipe, and all spatial resolutions (1, 0.5, and 0.2 m). All separate outputs are available in the Supplementary material together with those of the remaining scenarios

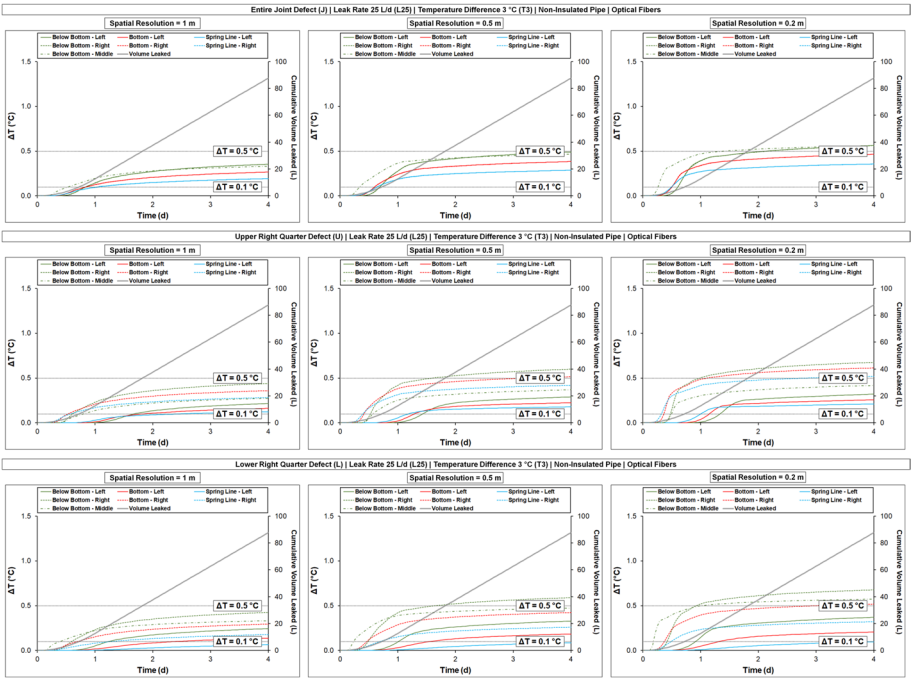

Fig. 8 Predicted temperature alterations over time with respect to the initial conditions (ΔT) at the optical fibers for all pipe defect configurations (J – entire joint defect, U – upper right quarter joint defect, L – lower right quarter joint defect), leak rate of 25 L/d (L25), temperature difference of 3 °C between leaked water and undisturbed soil (T3), non-insulated pipe, and all spatial resolutions (1, 0.5, and 0.2 m). All separate outputs are available in the Supplementary material together with those of the remaining scenarios

temperature alterations sooner than those at the left side. These alterations generally occur first at the optical fibers below the bottom of the pipe (middle and right), then at the bottom (right), at the spring line (right), and at the left side (below bottom first, then bottom, and spring line) as the leaks occur at the lower right quarter of the joint. Conversely, when the leaks occur at the upper right quarter of the joint, the optical fiber located at the spring line (right) is generally the first where a temperature alteration can be observed, then followed by the ones at the bottom (right) and below the bottom (right and middle), and by those at the left side (spring line first, then bottom, and below bottom).

Although temperature alterations can occur earlier at a specific location, it does not necessarily mean that here these alterations will be higher or that the selected detection thresholds (0.1 and 0.5 °C, Sec. 2.1) will be overcome earlier (Figs. 7, 8, 9 and 10; Supplementary material). Consistently with the flow and temperature fields described in the previous sections (Secs. 3.1 and 3.2), temperature alterations are generally higher at the optical fibers located below the bottom of the pipe, followed by those at the bottom, and at the spring line. The same applies when the leaks occur at the right side, although as expected the highest alterations are recorded by the optical fibers at this side. However, temperature alterations recorded at the left side can overcome the detection thresholds as well in these scenarios, especially below the bottom of the pipe.

Besides of the location of the optical fibers, the spatial resolution (Sec. 2.1) has an important role as well in determining whether recorded temperature alterations at the fibers

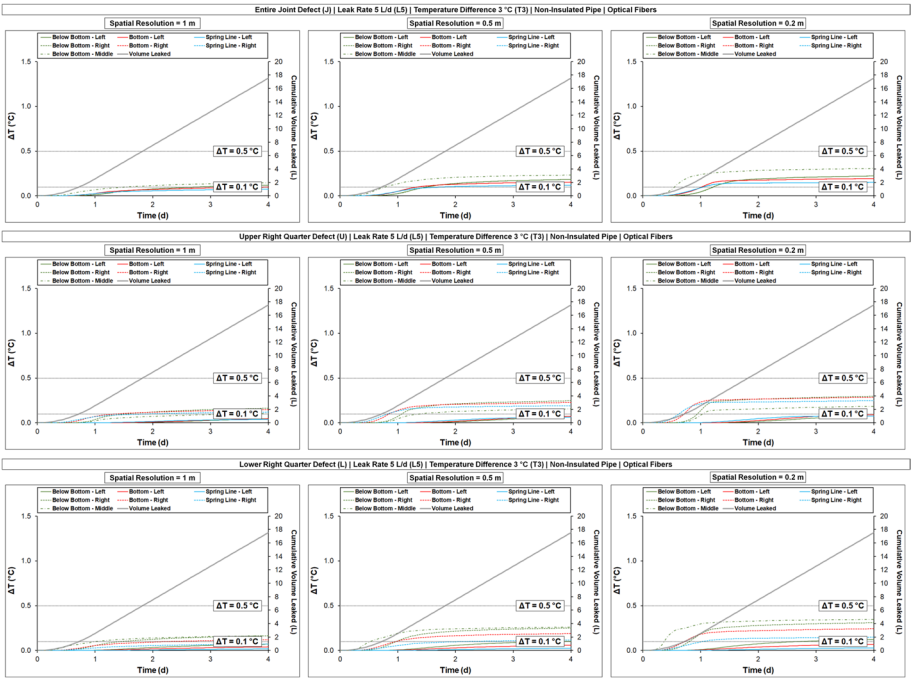

Fig. 9 Predicted temperature alterations over time with respect to the initial conditions (ΔT) at the optical fibers for all pipe defect configurations (J – entire joint defect, U – upper right quarter joint defect, L – lower right quarter joint defect), leak rate of 5 L/d (L5), temperature difference of 3 °C between leaked water and undisturbed soil (T3), non-insulated pipe, and all spatial resolutions (1, 0.5, and 0.2 m). All separate outputs are available in the Supplementary material together with those of the remaining scenarios

can overcome the selected detection thresholds. Indeed, as the spatial resolution becomes finer (i.e., from 1 to 0.2 m), the length over which modeled temperatures are averaged reduces, and recorded values inevitably deviate less between each other. As a result, temperature alterations recorded at the optical fibers become higher and occur more abruptly at the beginning, whereas their growth rate decreases more at later stages (Figs. 7, 8, 9 and 10; Supplementary material).

Temperature alterations at the optical fibers do not always overcome the detection thresholds in the time frame considered when the pipe is not thermally insulated (Figs. 7, 8 and 9; Supplementary material). Indeed, when the temperature difference between leaked water and the undisturbed soil is the lowest (1 °C), only the lowest detection threshold (0.1 °C) is overcome, and generally this occurs for the highest leak rate (125 L/d), where temperature alterations at the optical fibers reach a maximum of about 0.35 °C. Practically, no detection can occur for the lowest leak rate (5 L/d), where temperature alterations barely reach 0.1 °C with the finest spatial resolution (0.2 m). At 25 L/d, detection could occur only with the finest spatial resolution, where maximum temperature alterations at the optical fibers are around 0.2 – 0.25 °C. As the temperature difference between leaked water and the undisturbed soil increases up to 3 °C, it would be still difficult to detect leaks as low as 5 L/d, despite most of the time the 0.1 °C threshold is overcome (maximum alterations at the optical fibers of about 0.35 °C). However, depending on the scenarios the 0.5 °C detection threshold is now overcome at 25 L/d with both 0.5 and 0.2 m spatial

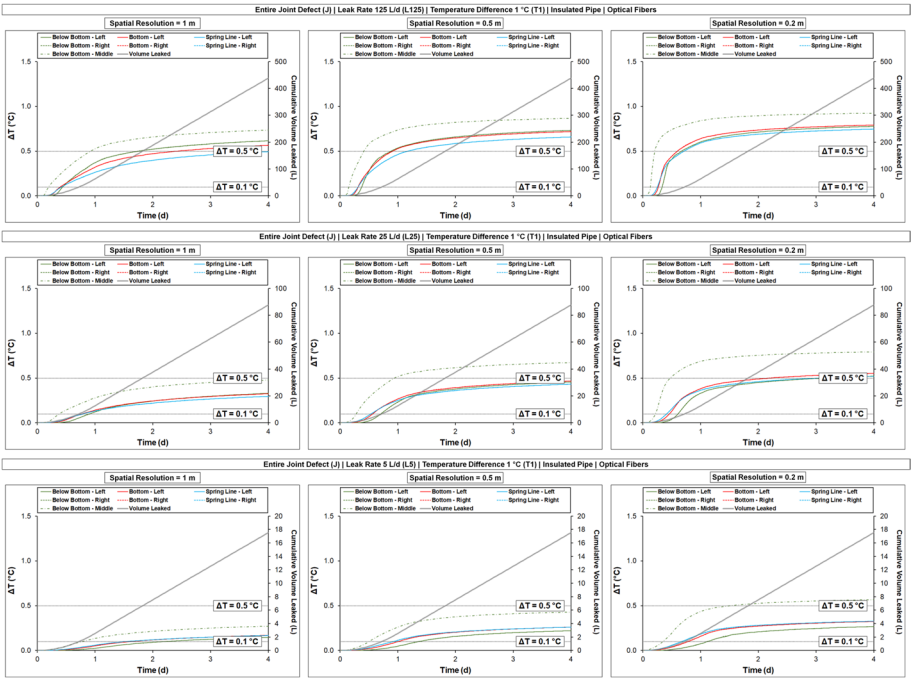

Fig. 10 Predicted temperature alterations over time with respect to the initial conditions (ΔT) at the optical fibers for the entire joint defect configuration (J), leak rates of 5, 25, and 125 L/d (L5, L25, and L125), temperature difference of 1 °C between leaked water and undisturbed soil (T1), insulated pipe (I), and all spatial resolutions (1, 0.5, and 0.2 m). All separate outputs are available in the Supplementary material together with those of the remaining scenarios

resolutions mostly at the optical fibers below and at the bottom of the pipe (maximum values around 0.56 – 0.68 °C). At 125 L/d, the maximum temperature alteration recorded at the optical fibers reaches roughly 1.05 °C, and the 0.5 °C threshold is overcome in all pipe defect configurations in around (and even before) 1 day with the coarsest spatial resolution (1 m), except for the optical fibers at the bottom and at the spring line on the left side when the leaks occur at the lower right quarter of the joint and at the upper right quarter (in the latter, the 0.5 °C threshold can still be overcome at these locations with finer spatial resolutions). It is also worth noting that now (at 125 L/d and 3 °C temperature difference with the undisturbed soil) temperature alterations occurring at the optical fiber below the bottom of the pipe on the left side are comparable in magnitude and detection time to those closer to the leaks when these occur on the right side. As the temperature difference between leaked water and the undisturbed soil reaches 5 °C, temperature alterations at the optical fibers always overcome the 0.1 °C detection threshold even at the lowest leak rate (5 L/d). However, at 5 L/d the 0.5 °C threshold is just slightly overcome or barely reached with the finest spatial resolution in the time frame considered (maximum alterations around 0.49 – 0.58 °C). At 25 L/d, the 0.5 °C threshold is overcome with a spatial resolution of 1 m already (mostly below the bottom of the pipe), although it is with finer spatial resolutions that temperature alterations overcome this threshold at most fibers (maximum values around 0.94 – 1.12 °C). Finally, at 125 L/d the outcome is similar to the scenarios with a 3 °C temperature difference between leaked water and the undisturbed soil, other than that

the 0.5 °C detection threshold is overcome much earlier with all spatial resolutions, and the maximum recorded alterations at the optical fibers reach values up to 1.6 and 1.75 °C.

When the pipe is thermally insulated, as expected temperature alterations at the optical fibers are much higher, even at very low leak rates and with just a 1 °C temperature difference between leaked water and the undisturbed soil. Indeed, in all these scenarios the 0.1 °C detection threshold is always overcome at all optical fibers with the coarsest spatial resolution (1 m). At 5 L/d, the 0.5 °C threshold is slightly overcome just below the bottom of the pipe (middle) with the finest spatial resolution (0.2 m). As the leak rate increases to 25 L/d, this threshold is overcome around 1 day below the bottom of the pipe (middle) with a 0.5 m spatial resolution, whereas at all optical fibers with the finest spatial resolution (maximum temperature alterations around 0.79 °C). At 125 L/d, temperature alterations overcome the 0.5 °C detection threshold at all fibers except at the spring line with the coarsest spatial resolution (1 m), where it occurs when this is finer (0.5 and 0.2 m). Maximum temperature alterations at the optical fibers here reach about 0.93 °C, almost equal to the maximum temperature difference at the joint defect (1 °C).

4 Discussion

4.1 Potential For Detecting, Locating, and Quantifying Background Leakages With Fiber Optic DTS

The analysis of flow and temperature alterations around the leaks (Sec. 3) showed that there is potential to use this information to detect and locate background leakages with fiber optic distributed temperature sensing. Strikingly, despite the influence of pipe temperature on the surrounding soil, noticeable temperature alterations can occur within the utility trench in the close vicinity of the leaks (up to 1.75 °C at about 22 cm from the pipe defect, namely at the optical fiber on the right side and below the bottom of the pipe), provided that the leak rate is not too small and that a sufficient temperature difference exists between leaked water and the undisturbed soil. Therefore, detectable temperature alterations in proximity to the leaks are not limited to the case of a thermally insulated pipe, where even a 1 °C difference between leaked water and the undisturbed soil could be sufficient to overcome detection thresholds (Sec. 3). Indeed, in absence of thermal insulation, the modeled scenarios showed that temperature alterations resulting from leaks as small as 125 L/d and with a temperature difference of 3 – 5 °C with the undisturbed soil substantially overcome the detection threshold of 0.5 °C in short time (around 1 day) with a coarse spatial resolution (1 m) of the sensing system and, therefore, could be detected. It is not unlikely that leaks of this magnitude could overcome this detection threshold even with a temperature difference lower than 3 °C between leaked water and the undisturbed soil, given that temperature alterations at the optical fibers can still reach maximum values of about 0.35 °C when the temperature difference with the undisturbed soil drops to 1 °C (Sec. 3). Leaks as low as 25 L/d overcome the 0.5 °C detection threshold and could be detected as well but with finer spatial resolutions and with temperature differences between leaked water and the undisturbed soil ≥ 3 °C. At 5 L/d, detection becomes practically impossible unless the 0.1 °C detection threshold and finer spatial resolutions are considered. However, it would be very unlikely to detect a leak by relying on such a small detection threshold for a water infrastructure, since it would be hard to discriminate such small leak-induced temperature alterations even from natural temperature fluctuations of

water within the pipes. Furthermore, relatively coarse spatial and temperature resolutions (1 – 0.5 m, 0.1 °C) are currently preferred for practical applications of kilometers long infrastructure in order to reduce acquisition times and data storage, which would otherwise become demanding.

Despite not all modeled leaks are deemed potentially detectable with fiber optic DTS, the results previously described are promising. Indeed, it is important to stress that modeled leak rates (5, 25, and 125 L/d) are extremely small for a single pipe defect in a water infrastructure and that could not be detected otherwise. To give a practical figure of how small these leak rates are, it would take around 58 min to fill a disposable cup of 200 mL at 5 L/d, 12 min at 25 L/d, and 2 min at 125 L/d. However, although small, these leak rates are fully representative of background leakages, which are ubiquitous in real water infrastructure. Therefore, modeling temperature alterations high enough to make these small leaks potentially detectable with optical fibers might open up new possibilities in the challenge of detecting and locating a wide range of leakages in water infrastructure, especially background leakages, which are responsible for large amounts of water lost and run undetected with the technologies used in the current practice. These results can also potentially dispel the common assumption that temperature alterations induced by small leakages with small to moderate temperature differences with the surrounding soil/trench filling material are negligible in the close vicinity of buried water pipelines without thermal insulation, thus laying the groundwork for a more conscious application of DTS systems in water infrastructure.

Numerical results also showed a clear nonlinear relationship between volume leaked and temperature alterations at the optical fibers ("cumulative volume leaked" versus "temperature alterations" curves in the Supplementary material). These curves are not reported in Section 3 as they have practically the same behavior of those describing temperature alterations over time at the optical fibers (Figs. 7, 8, 9 and 10; Supplementary material) and the same considerations can be drawn, except for a slightly higher nonlinearity during the first day as the volume of leaked water varies nonlinearly here (simply because the leak rate varies linearly). These curves could be derived in practical applications as well with proper calibration of a modeling framework like the one used in the current work supported by a series of DTS recordings, thus also enabling leakages quantification along the entire sensing cable.

4.2 Optical Fibers Location for New and Existing Water Pipelines

Within the utility trench, the part below the bottom of the pipe showed overall higher temperature alterations and faster detection times in response to modeled leaks (Sec. 3). Therefore, this would likely be the best location to place an optical fiber to detect and locate water leakages with DTS, provided that a sufficient distance from the pipe can be established (between 10 and 22 cm in the modeled scenarios). Strikingly, it would not be necessary to place the optical fiber directly below the pipe (i.e., along its vertical centerline), as it is generally suggested for liquid pipelines (Inaudi et al. 2008), or even in a separate trench beneath the one hosting the pipe, as suggested by other technical guidelines (Ziemendorff 2022). Indeed, optical fibers located at the sides of the pipe and below its bottom showed comparable or even better performance (the latter for the highest leak rate modeled, 125 L/d) in terms of temperature alterations and detection times. This means that this technology could be used to retrofit existing pipelines as well while reducing installation and maintenance costs, since it would not be strictly required to place the optical fiber directly below the pipe, which would be feasible for new pipelines only.

Although locating the optical fiber in a separate trench (Ziemendorff 2022) would increase its distance from the pipeline, thus reducing the influence of pipe temperature, it would be more expensive and could also be counterproductive. Indeed, if the backfill of this additional trench is made of a cohesionless free draining material (i.e., sand/gravel), like the one generally used for the utility trench hosting the pipe, in the unsaturated zone this trench will likely act as a capillary barrier (Ross 1990; Oldenburg and Pruess 1993), locally diverting water leaked from the overlying pipe, as shown by D'Aniello et al. (2022) for a similar setting. Therefore, unless breakthrough occurs within this additional trench, leaked water would not reach the optical fiber, and detection would be hardly possible.

As a final remark, the utility trench itself could also act as a capillary barrier, but with respect to infiltrated stormwater. However, if the optical fiber is located within the same trench of the pipe, in this case this would be beneficial as it would prevent stormwater from reaching the optical fiber and from temporarily altering recorded temperatures (again, unless breakthrough occurs, which would depend on soil properties and stormwater infiltration rates). The effects of infiltrated stormwater on recorded temperatures are well documented by Jacobsz and Jahnke (2020) in their long-term field scale experiment.

5 Conclusions

In this study, a detailed analysis of flow and temperature alterations around a leaking water pipeline buried in the subsurface was presented for the first time to test the feasibility of detecting and locating background leakages with fiber optic distributed temperature sensing (DTS). Transient 3D heat transfer-unsaturated flow numerical simulations showed that noticeable temperature alterations can occur within the utility trench in the close vicinity of the leaks despite the influence of pipe temperature on the surrounding soil, and that extent, distribution, and magnitude of these alterations are convection dominated at a given temperature difference between leaked water and undisturbed soil. When the pipe is thermally insulated, predicted temperature alterations at the optical fibers located within the utility trench overcome the 0.5 °C detection threshold in most scenarios even at a 1 °C difference between leaked water and the undisturbed soil. Conversely, in absence of thermal insulation, the modeled scenarios showed that: i) leaks as small as 125 L/d and with a temperature difference of 3 – 5 °C (and likely lower) with the undisturbed soil could be detected, as the resulting temperature alterations at the optical fibers substantially overcome the detection threshold of 0.5 °C in short time (around 1 day) with a coarse spatial resolution (1 m) of the sensing system; ii) leaks as low as 25 L/d could be detected as well but only with finer spatial resolutions (0.5 and 0.2 m) and with temperature differences between leaked water and the undisturbed soil $\geq$ 3 °C; iii) leaks of 5 L/d would be practically impossible to detect unless a lower detection threshold (0.1 °C) and fine spatial resolutions are considered.

The analysis is also the first to suggest that it may not be strictly necessary to place the optical fiber directly below the pipe (i.e., along its vertical centerline) or in a separate trench beneath the one hosting the pipe, which may be counterproductive as the additional trench could act as a capillary barrier with respect to leaked water. Indeed, optical fibers located within the utility trench at the sides of the pipe and below its bottom showed comparable or even better performance in terms of temperature alterations and detection times in all pipe defect configurations (i.e., entire joint, upper right quarter, and lower right quarter joint defects). Therefore, retrofitting existing pipelines with a fiber optic DTS technology could

become a competitive and viable option as the optical fiber would not be directly placed below the pipe, feasible for new pipelines only.

Overall, this analysis is the first to show that there is potential to use temperature alterations around water pipelines (with or without thermal insulation) to detect and locate incredibly small leaks with fiber optic DTS, and it is the first contribution to dispel the common assumption that temperature alterations induced by small leakages with small to moderate temperature differences with the surrounding soil are negligible in the close vicinity of buried pipes. Indeed, modeled leak rates are representative of background leakages, which could not be detected otherwise. Leaks quantification could also be possible along the sensing cables since numerical simulations further showed the occurrence of clear nonlinear relationships between volume leaked and temperature alterations at the optical fibers.

The outcomes of this research are promising, but further experimental and field evidence is required. However, the new theoretical and practical insights gained will surely help practitioners, researchers, and the whole water industry in this endeavor, creating new possibilities for detecting, locating, and quantifying leakages, still an open challenge for a more sustainable urban environment.

Supplementary material Supplementary material to this article can be found at https://doi.org/10.6084/m9.figshare.21909396.

Appendix

Governing Equations: Unsaturated Flow in Porous Media

By default, the Richards' Equation interface (Subsurface Flow module) of COMSOL Multiphysics® version 6.0.0.405 solves the pressure-based formulation of Richards' equation by the finite element method (Bear 1972; Istok 1989; COMSOL 2021). However, to account for fluid properties variation with temperature without resorting to the Oberbeck-Boussinesq approximation (Nield and Bejan 2013), the standard formulation employed by COMSOL was modified to avoid the expansion of the time derivative (i.e., the storage term), so as to obtain the generalized form of the equation of transient groundwater flow through variably water saturated porous media (Bear 1972; Istok 1989):

$$\frac{\partial \rho_w \theta_w}{\partial t} - \nabla \cdot \left[\frac{\rho_w k k_{rw}}{\mu_w} \left(\nabla p_w - \rho_w \underline{g} \right) \right] = Q_w \tag{1}$$

with $\theta_w = S_w \phi$ the soil water content, S_w the water saturation, ϕ the porosity, p_w the water pressure, k the intrinsic permeability (a scalar or a tensor depending on the presence of anisotropy), k_{rw} the relative permeability, ρ_w the water density, μ_w the water dynamic viscosity, $\underline{g}$ the gravity vector, and Q_w the water mass rate per unit volume (source/sink term). Water saturation S_w is expressed as a function of the effective water saturation $\overline{S}_w = \frac{S_w - S_{w,r}}{1 - S_{w,r}}$, which varies between 0 and 1. If the soil is fully water saturated ($S_w = 1$), water content equals porosity and is referred to as saturated water content θ_s, whereas if the soil is at its residual water saturation ($S_w = S_{w,r}$), it is referred to as residual water content θ_r.

The soil capillary pressure–saturation constitutive relationship is defined according to the van Genuchten retention curve (van Genuchten 1980):

$$\overline{S}_w = \left[\frac{1}{1+\left(\alpha h_{aw}\right)^n}\right]^m \tag{2}$$

with h_{aw} the capillary pressure head between air (subscript a) and water (subscript w), namely $h_{aw} = h_a - h_w = -h_w = -\frac{p_w}{\rho_w g}$ (as $h_a = 0$ under the basic assumptions of groundwater flow through variably water saturated porous media) being h the pressure head and g the gravitational constant, α and n the van Genuchten parameters, and $m = 1 - 1/n$ with $n > 1$ according to Mualem's model (Mualem 1976).

Relative permeability is related to the hydraulic conductivity $K_w = k_{rw} K_{sw}$, with $K_{sw} = \frac{\rho_w g}{\mu_w} k$ the saturated hydraulic conductivity, and is expressed with the van Genuchten–Mualem function (Mualem 1976; van Genuchten 1980):

$$k_{rw} = \overline{S}_w^{\,1/2}\left[1 - \left(1 - \overline{S}_w^{\,1/m}\right)^m\right]^2 \tag{3}$$

which varies from 0 ($\overline{S}_w = 0$) to 1 ($\overline{S}_w = 1$).

Governing Equations: Heat Transfer in Porous Media

Under the assumption of local thermal equilibrium, the Heat Transfer in Porous Media interface (Heat Transfer module) of COMSOL Multiphysics® version 6.0.0.405 solves the following form of the heat equation by the finite element method (Nield and Bejan 2013; COMSOL 2021):

$$(\rho c)_e \frac{\partial T}{\partial t} + \rho_w c_{p,w} \underline{u} \cdot \nabla T - \nabla \cdot \left(k_e \nabla T\right) = Q \tag{4}$$

with $(\rho c)_e$ the effective heat capacity per unit volume, T the temperature, ρ_w the water density, $c_{p,w}$ the water specific heat at constant pressure, $\underline{u}$ the apparent groundwater velocity field, k_e the effective thermal conductivity (a scalar or a tensor depending on the presence of anisotropy), and Q the heat rate per unit volume (source/sink term).

For a variably water saturated porous medium, the effective heat capacity per unit volume becomes:

$$(\rho c)_e = (1-\phi)\rho_s c_s + \theta_w \rho_w c_{p,w} + \theta_a \rho_a c_{p,a} \tag{5}$$

whereas the effective thermal conductivity, assuming heat conduction occurring in parallel in the solid and fluid phases:

$$k_e = (1-\phi)k_s + \theta_w k_w + \theta_a k_a \tag{6}$$

with ϕ the porosity, ρ_s the solid phase density, c_s the solid phase specific heat, θ_w the soil water content, θ_a the soil air content, ρ_a the air density, $c_{p,a}$ the air specific heat at constant pressure, k_s the solid phase thermal conductivity, k_w the water thermal conductivity, and k_a the air thermal conductivity. In presence of thermal dispersion, the term $k_d = \rho_w c_{p,w} D_{ij}$ is added to the right-hand side of (6), with $D_{ij} = \lambda_{ijkl} \frac{v_k v_l}{|\underline{v}|}$ the dispersion tensor, λ_{ijkl} the dispersivity tensor (Nield and Bejan 2013; COMSOL 2021), $\underline{v} = \underline{u}/\theta_w$ and v_k, v_l the pore water velocity field and its components.

Acknowledgements The author wishes to thank Prof. Domenico Pianese for his trust and encouragement.

Author Contributions The author (AD) confirms that he is solely responsible for this study.

Funding Open access funding provided by Università degli Studi di Napoli Federico II within the CRUI-CARE Agreement. The author declares that no funds, grants, or other support were received during the preparation of this manuscript.

Availability of Data and Materials All data supporting this study are available within the manuscript.

Declarations

Ethical Approval Not applicable.

Consent to Participate Not applicable.

Consent to Publish Not applicable.

Competing Interests The author has no financial or non-financial interests to disclose.

References

Adedeji KB, Hamam Y, Abe BT, Abu-Mahfouz AM (2017) Towards achieving a reliable leakage detection and localization algorithm for application in water piping networks: An overview. IEEE Access 5:20272–20285

Attard G, Winiarski T, Rossier Y, Eisenlohr L (2016) Impact of underground structures on the flow of urban groundwater. Hydrogeol J 24(1):5–19

Bear J (1972) Dynamics of fluids in porous media. Dover Publications Inc, New York

Bhaskar AS, Beesley L, Burns MJ, Fletcher TD, Hamel P, Oldham CE, Roy AH (2016) Will it rise or will it fall? Managing the complex effects of urbanization on base flow. Freshw Sci 35(1):293–310

Bolognini G, Hartog A (2013) Raman-based fibre sensors: Trends and applications. Opt Fiber Technol 19(6):678–688

Burri NM, Weatherl R, Moeck C, Schirmer M (2019) A review of threats to groundwater quality in the anthropocene. Sci Total Environ 684:136–154

Carsel RF, Parrish RS (1988) Developing joint probability distributions of soil water retention characteristics. Water Resour Res 24(5):755–769

Chisala BN, Lerner DN (2008) Distribution of sewer exfiltration to urban groundwater. Proc Instn Civ Engrs-Wat M 161(6):333–341

COMSOL (2021) Subsurface Flow Module User's Guide – Version 6.0. COMSOL Multiphysics. https://doc.comsol.com. Accessed 20 Sept 2022

Dalla Santa G, Galgaro A, Sassi R, Cultrera M, Scotton P, Mueller J, Bernardi A (2020) An updated ground thermal properties database for GSHP applications. Geothermics 85:101758

D'Aniello A, Cimorelli L, Pianese D (2021) Leaking pipes and the urban karst: a pipe scale numerical investigation on water leaks flow paths in the subsurface. J Hydrol 603:126847. https://doi.org/10.1016/j.jhydrol.2021.126847

D'Aniello A, Cimorelli L, Pianese D (2022) Utility trenches: sinks or barriers? Modeling the fate of leaked water in a crowded subsurface. J Hydrol 612:128303. https://doi.org/10.1016/j.jhydrol.2022.128303
Diersch HJG (2014) FEFLOW: Finite Element Modeling of Flow, Mass and Heat Transport in Porous and Fractured Media. Springer-Verlag Berlin Heidelberg
Drusová S, Bakx W, Doornenbal PJ, Wagterveld RM, Bense VF, Offerhaus HL (2021) Comparison of three types of fiber optic sensors for temperature monitoring in a groundwater flow simulator. Sens Actuator A Phys 331:112682
FAO – Food and Agriculture Organization of the United Nations (2012) Coping with water scarcity – An action framework for agriculture and food security. FAO Water Reports 38, Rome
Foster SSD (2001) The interdependence of groundwater and urbanisation in rapidly developing cities. Urban Water 3(3):185–192
Han D, Currell MJ, Cao G, Hall B (2017) Alterations to groundwater recharge due to anthropogenic landscape change. J Hydrol 554:545–557
Hibbs BJ, Sharp JM Jr (2012) Hydrogeological impacts of urbanization. Environ Eng Geosci 18(1):3–24
Howard AK (1996) Pipe Bedding and Backfill. Geotechnical Training Manual No. 7, United States Department of the Interior, Bureau of Reclamation, Technical Service Center, Geotechnical Services, Denver, Colorado
Hu Z, Chen B, Chen W, Tan D, Shen D (2021) Review of model-based and data-driven approaches for leak detection and location in water distribution systems. Water Supply 21(7):3282–3306
Ibrahim K, Tariq S, Bakhtawar B, Zayed T (2021) Application of fiber optics in water distribution networks for leak detection and localization: a mixed methodology-based review. H2 Open J 4(1):244–261
Inaudi D, Belli R, Walder R (2008) Detection and localization of micro-leakages using distributed fiber optic sensing. International Pipeline Conference 48579:599–605
Istok JD (1989) Groundwater modelling by the finite element method. Water Resources Monograph, 13, American Geophysical Union (2000) Florida Avenue. NW, Washington, DC, p 2000
Jacobsz SW, Jahnke SI (2020) Leak detection on water pipelines in unsaturated ground by discrete fibre optic sensing. Struct Health Monit 19(4):1219–1236
Lambert A, Trow S, Merks C, Charalambous B, Donnelly A, Galea St John S, Fantozzi M, Hulsmann A, Koelbl J, Kovač J, Schipper D (2015a) EU Reference Document Good Practices on Leakage Management WFD CIS WG PoM – Main Report. Office for Official Publications of the European Communities, Luxembourg, European Union
Lambert A, Trow S, Merks C, Charalambous B, Donnelly A, Galea St John S, Fantozzi M, Hulsmann A, Koelbl J, Kovač J, Schipper D (2015b) EU Reference Document Good Practices on Leakage Management WFD CIS WG PoM – Case Study document. Office for Official Publications of the European Communities, Luxembourg, European Union
Lambert AO (2009) Ten years experience in using the UARL formula to calculate infrastructure leakage index. International Water Association (IWA) Waterloss 2009 Conference, Cape Town, South Africa
Lambert AO, Brown TG, Takizawa M, Weimer D (1999) A review of performance indicators for real losses from water supply systems. J Water SRT – Aqua 48(6):227–237
Lambert AO, McKenzie R (2002) Practical experience in using the Infrastructure Leakage Index. International Water Association (IWA) Conference "Leakage Management: A Practical Approach." Lemesos, Cyprus
Lerner DN (1986) Leaking Pipes Recharge Ground Water Groundwater 24(5):654–662
Lerner DN (1990) Groundwater recharge in urban areas. Atmos Environ 24B(1):29–33
Lerner DN (2002) Identifying and quantifying urban recharge: a review. Hydrogeol J 10(1):143–152
Li R, Huang H, Xin K, Tao T (2015) A review of methods for burst/leakage detection and location in water distribution systems. Water Sci Technol Water Supply 15(3):429–441
Liemberger R, Wyatt A (2019) Quantifying the global non-revenue water problem. Water Supply 19(3):831–837
Lombera RR, Serrano JM, Martinez O, San Emeterio JD, Lopez-Higuera JM (2014) Experimental demonstration of a leakage monitoring system for large diameter water pipes using a fiber optic distributed sensor system. In SENSORS, 2014 IEEE Conference 1885–1888
Milano V (2012) Acquedotti – Guida alla progettazione. Hoepli Editore, Milano
Motil A, Bergman A, Tur M (2016) State of the art of Brillouin fiber-optic distributed sensing. Opt Laser Technol 78:81–103
Mualem Y (1976) A new model for predicting the hydraulic conductivity of unsaturated porous media. Water Resour Res 12(3):513–522
Nield DA, Bejan A (2013) Convection in Porous Media. Springer Science+Business Media, New York

Niklès M, Vogel BH, Briffod F, Grosswig S, Sauser F, Luebbecke S, Pfeiffer T (2004) Leakage detection using fiber optics distributed temperature monitoring. In Smart Structures and Materials 2004: Smart Sensor Technology and Measurement Systems. Proceedings of SPIE 5384:18–25

Oldenburg CM, Pruess K (1993) On numerical modeling of capillary barriers. Water Resour Res 29(4):1045–1056

Price M, Reed DW (1989) The influence of mains leakage and urban drainage on groundwater levels beneath conurbations in the UK. Proc Instn Civ Engrs 86(1):31–39

Ross B (1990) The diversion capacity of capillary barriers. Water Resour Res 26(10):2625–2629

Stokes CS, Simpson AR, Maier HR (2014) The cost–greenhouse gas emission nexus for water distribution systems including the consideration of energy generating infrastructure: an integrated conceptual optimization framework and review of literature. Earth Perspectives 1(1):1–17

The Engineering ToolBox (2001) Free tools and information for engineering and design of technical applications. https://www.engineeringtoolbox.com/. Accessed 7 Oct 2022

Tubau I, Vázquez-Suñé E, Carrera J, Valhondo C, Criollo R (2017) Quantification of groundwater recharge in urban environments. Sci Total Environ 592:391–402

United States Department of Agriculture Soil Conservation Service – USDA SCS (1987) Soil Mechanics Level 1, Module 3 – USDA Soil Textural Classification, Study Guide. USDA Soil Conservation Service, Washington DC

van Genuchten MT (1980) A closed-form equation for predicting the hydraulic conductivity of unsaturated soils. Soil Sci Soc Am J 44(5):892–898

Vázquez-Suñé E, Sánchez-Vila X, Carrera J (2005) Introductory review of specific factors influencing urban groundwater, an emerging branch of hydrogeology, with reference to Barcelona. Spain Hydrogeol J 13(3):522–533

Wakida FT, Lerner DN (2005) Non-agricultural sources of groundwater nitrate: a review and case study. Water Res 39(1):3–16

Waltham T, Bell FG, Culshaw MG (2005) Sinkholes induced by engineering works. In: Sinkholes and Subsidence: Karst and Cavernous Rocks in Engineering and Construction. Springer, Berlin, Heidelberg

Wang L, Narasimman SC, Ravula SR, Ukil A (2017) Water ingress detection in low-pressure gas pipelines using distributed temperature sensing system. IEEE Sens J 17(10):3165–3173

Wang Q, Gu X, Zhang Z, Long Z, Zhao Y (2022) On-Line Leakage Detection in Buried Tap Water Distribution Pipes Using Distributed Temperature Sensing. J Pipeline Syst Eng Pract 13(2):04022010

Yorkshire Water (2018) Mains Design and Construction Guidelines for Self-Lay Providers. https://www.yorkshirewater.com/. Accessed 4 Oct 2022

Wijaya H, Rajeev P, Gad E (2021) Distributed optical fibre sensor for infrastructure monitoring: Field applications. Opt Fiber Technol 64:102577

Wu J, Nofziger DL (1999) Incorporating temperature effects on pesticide degradation into a management model. J Environ Qual 28(1):92–100

Xu Y, Li J, Zhang M, Yu T, Yan B, Zhou X, ... Gao S (2020) Pipeline leak detection using Raman distributed fiber sensor with dynamic threshold identification method. IEEE Sens J 20(14):7870–7877

Ziemendorff S (2022) Comparison of suitable leak detection methods. Selection Guideline with special consideration of the conditions in countries with emerging markets and developing economies. Deutsche Gesellschaft für Internationale Zusammenarbeit (GIZ) GmbH, 1st Edition, Eschborn. https://doi.org/10.5281/zenodo.6625858